Bimetallic Au–Ni Nanoparticles Embedded in SiO$_2$ Nanospheres: Synergetic Catalysis in Hydrolytic Dehydrogenation of Ammonia Borane

Hai-Long Jiang,[a, c] Tetsuo Umegaki,[a] Tomoki Akita,[a, c] Xin-Bo Zhang,[a] Masatake Haruta,[b, c] and Qiang Xu*[a, c]

Abstract: Gold–nickel nanoparticles (NPs) of 3–4 nm diameter embedded in silica nanospheres of around 15 nm have been prepared by using [Au(en)$_2$Cl$_3$] and [Ni(NH$_3$)$_6$Cl$_2$] as precursors in a NP-5/cyclohexane reversed-micelle system, and by in situ reduction in an aqueous solution of NaBH$_4$/NH$_3$BH$_3$. Compared with monometallic Au@SiO$_2$ and Ni@SiO$_2$, the as-synthesized Au–Ni@SiO$_2$ catalyst shows higher catalytic activity and better durability in the hydrolysis of ammonia borane, generating a nearly stoichiometric amount of hydrogen.

Keywords: dehydrogenation · gold · heterogeneous catalysis · nanoparticles · nickel

During the generation of H$_2$, the synergy effect between gold and nickel is apparent: The nickel species stabilizes the gold NPs and the existence of gold helps to improve the catalytic activity and durability of the nickel NPs.

Introduction

Global energy consumption is expected to increase steadily in the next few decades. Hydrogen is one of the energy carriers that is useful for energy saving and conservation of the global environment. To meet the US Department of Energy (DOE) target for on-board applications, hydrogen storage materials must have a low weight and high gravimetric hydrogen storage capacity with a rapid hydrogen release rate. There have been a large number of reports on hydrogen-storage materials[1,2] and on on-board reforming of hydrocarbons to yield hydrogen.[3] However, big challenges still remain. Among the potential candidates for effective chemical hydrogen storage, ammonia borane (AB; NH$_3$BH$_3$) has a hydrogen content of 19.6 wt %, which exceeds that of gasoline, and is accordingly an attractive candidate for chemical hydrogen-storage applications.[4–6] The development of efficient catalysts to further improve the kinetic properties in the hydrolytic dehydrogenation of ammonia borane under moderate conditions is therefore important for the practical application of this system.[5] We have thus been exploring low-cost and high-efficiency catalysts and are systematically investigating nickel-based catalysts that exhibit high efficiency in hydrogen generation.[7]

On the other hand, catalysis by gold nanoparticles (NPs) has attracted increasing attention because supported gold catalysts have been found to have a surprisingly high activity in CO oxidation.[8] The catalytic activity depends not only on the size of the gold nanoparticles, but also on the nature of the support and even the preparation methods of the catalysts.[9–11] Compared with those metal oxides with high isoelectric points (IEPs), for example, TiO$_2$, Fe$_2$O$_3$, and Co$_3$O$_4$, it is generally accepted that silica is an inert support and gold NPs are prone to aggregate due to their weak interactions with the surface of SiO$_2$. Many approaches have been developed for solving this problem, most often confining gold NPs within mesoporous silica,[12–14] modifying the silica support,[15] or alloying gold with a second metal.[16] Recently, different routes have been developed for coating gold NPs with silica to form well-dispersed silica nanospheres. However, as far as we know, all the gold NPs produced so far are still larger than 10 nm to date.[17,18]

[a] Dr. H.-L. Jiang, Dr. T. Umegaki, Dr. T. Akita, Dr. X.-B. Zhang, Prof. Dr. Q. Xu
National Institute of Advanced Industrial Science and Technology (AIST)
Ikeda, Osaka 563-8577 (Japan)
Fax: (+81) 72-751-7942
E-mail: q.xu@aist.go.jp

[b] Prof. Dr. M. Haruta
Graduate School of Urban Environmental Sciences
Tokyo Metropolitan University
Hachioji, Tokyo 192-0397 (Japan)

[c] Dr. H.-L. Jiang, Dr. T. Akita, Prof. Dr. M. Haruta, Prof. Dr. Q. Xu
CREST, Japan Science and Technology Agency (JST)
Kawaguchi, Saitama 332-0012 (Japan)

In this work, to address the problem of gold aggregation on the surface of silica, we have adopted two strategies that are executed simultaneously: Coating the gold NPs with silica and stabilizing them with nickel species. Herein, for the first time, we report the preparation of core–shell-structured Au–Ni@SiO$_2$ nanospheres with small Au–Ni particles (3–4 nm diameter) by a reversed-micelle method and by in situ reduction in an aqueous NaBH$_4$/NH$_3$BH$_3$ solution. The nickel-stabilized gold NPs exhibit remarkable resistance to aggregation and maintain their original sizes even after the generation of hydrogen. Moreover, the catalyst shows high activity towards hydrolytic dehydrogenation of ammonia borane and is recyclable. For comparison, the corresponding core–shell-structured Ni@SiO$_2$ and Au@SiO$_2$ nanospheres were also prepared by an analogous method. The nickel-free gold NPs show a high propensity towards coalescence and much lower catalytic activity, whereas the monometallic nickel catalyst exhibits poor durability. To the best of our knowledge, this is the first report of small Au–Ni NPs as cores within silica nanospheres prepared by a facile synthesis and of gold and nickel acting synergetically to catalyze the hydrolytic dehydrogenation of NH$_3$BH$_3$ with high activity.

Results and Discussion

Powder X-ray diffraction (XRD) was performed on all the as-synthesized core–shell-structured nanospheres. The strong and broad peaks in the range of $2\theta = 15$–$35°$ can be assigned to amorphous SiO$_2$ with no nickel or gold diffractions being detected in the XRD profiles (Figure 1), probably due to the nickel and gold loadings being too low or because the gold or nickel or Au–Ni particles are too small. The latter is supported by TEM observations for all these samples (Figure 2 and the Supporting Information). The TEM images (Figure 2) of the Au–Ni@SiO$_2$ sample reveal that the core–shell structures consist of well-proportioned spherical particles of silica of 15–20 nm diameter in which Au–Ni NPs of around 3–4 nm are embedded in the center of these SiO$_2$ spheres. It is assumed that the nucleation and
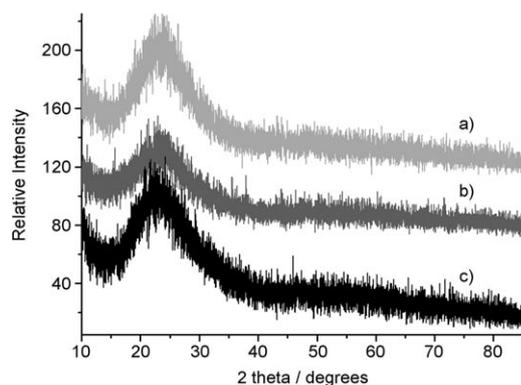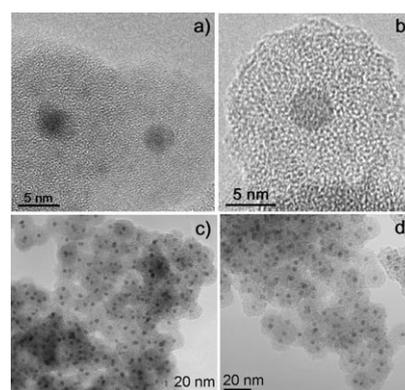

Figure 2. Representative high-magnification (a, b) and low-magnification (c, d) TEM images of the as-synthesized Au–Ni@SiO$_2$ nanospheres.

growth of metal–ammine complexes in the reversed-micelle system are responsible for the formation of the core–shell structures. Metal supported on SiO$_2$ was obtained when metal chloride was used in place of the metal–ammine complex as a precursor.[19] To increase the understanding of the form of nickel and gold, high-angle annular dark-field scanning transmission electron microscopy (HAADF-STEM) combined with energy-dispersive X-ray (EDX) spectrometry experiments were carried out. As can be seen from Figure 3 (left), there are many spherical substances with diameters of around 15 nm containing white spots with diameters of 2–4 nm. The EDX spectra (Figure 3, right) for points 3–7
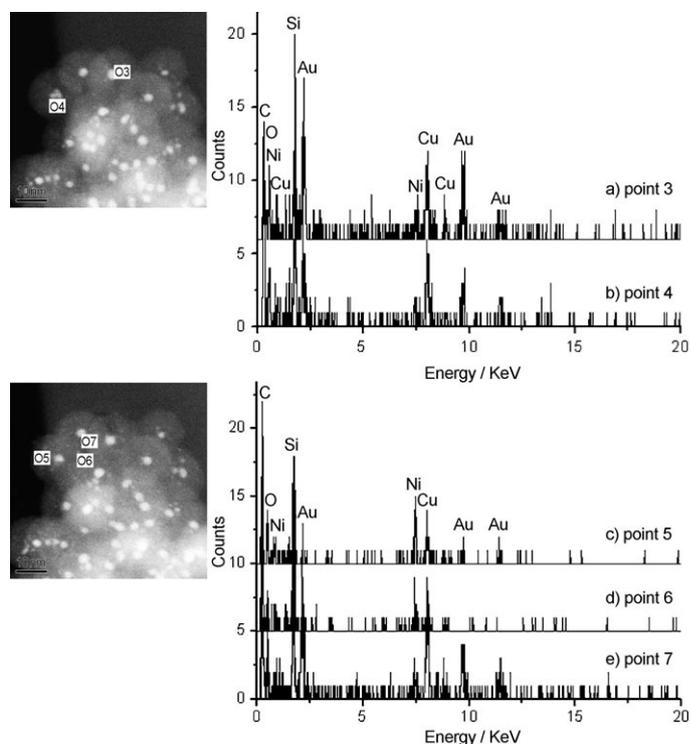

Figure 1. Powder XRD profiles for the as-synthesized a) Ni@SiO$_2$, b) Au@SiO$_2$, and c) Au–Ni@SiO$_2$ nanospheres.

Figure 3. HAADF-STEM images (left) and the corresponding EDX spectra (right) for the as-synthesized Au–Ni@SiO$_2$ nanospheres.

marked on the left-hand side of Figure 3 exhibit the following features. 1) The EDX spectra of all the white spots exhibit peaks corresponding to both gold (M and Lα peaks) and nickel (Kα and Lα peaks) elements, although the ratios of these peaks for each particle are not absolutely uniform. This shows that gold and nickel coexist in each spot/particle, but are not separate. 2) Most of the bimetallic NPs are located in the center of the SiO$_2$ spheres, whereas a few much smaller NPs are displaced from the center.

The as-synthesized nanospheres with different metal NPs in the core show distinct catalytic activities in the hydrolytic dehydrogenation of ammonia borane. Figure 4 shows the
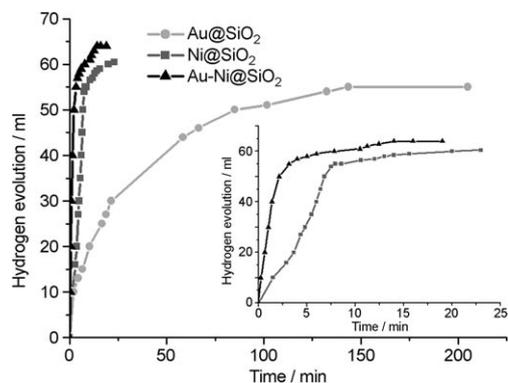

Figure 4. Generation of hydrogen by the hydrolysis of ammonia borane (AB, 0.152 M, 5 mL) in the presence of the as-synthesized Ni@SiO$_2$, Au@SiO$_2$ and Au–Ni@SiO$_2$ catalysts (Au/AB = 0.019, Ni/AB = 0.065) at 18 °C in air (inset: enlarged curves for Ni@SiO$_2$ and Au–Ni@SiO$_2$).

Figure 5. Hydrogen generation by hydrolysis of aqueous AB (0.152 M, 5 mL) catalyzed by a) Ni@SiO$_2$ and b) Au–Ni@SiO$_2$ in the presence and absence of NaBH$_4$.

time course of the hydrogen evolution from an aqueous solution of NH$_3$BH$_3$ in the presence of Ni@SiO$_2$, Au@SiO$_2$, and Au–Ni@SiO$_2$ catalysts and a small amount of NaBH$_4$. The reaction rate and the amount of hydrogen evolution depend significantly on the catalyst. The evolution of 60.5, 55.0, and 64.0 mL of hydrogen was completed in 23, 143, and 14 min, respectively, in the presence of the Ni@SiO$_2$, Au@SiO$_2$, and Au–Ni@SiO$_2$ catalysts.

As shown in Figure 5a, in the absence of NaBH$_4$, ammonia borane with the Ni@SiO$_2$ catalyst produced several milliliters of hydrogen at the onset of the reaction but produced only negligible H$_2$ after 1 min, which indicates that NaBH$_4$ is required to activate the catalyst/catalytic reaction. The effect of NaBH$_4$ on an iron catalyst in the hydrolysis of ammonia borane has also been reported.[5a] However, it is interesting that hydrogen can be produced from NH$_3$BH$_3$ catalyzed by Au–Ni@SiO$_2$ even in the absence of NaBH$_4$ (Figure 5b) although the activity is not as high as that in the presence of NaBH$_4$. These results indicate that the gold component in the catalyst not only improves the catalytic activity, but also plays a role in the activation of the catalyst. In the reaction system reported herein NaBH$_4$ was mixed with H$_2$O, NH$_3$BH$_3$, and the catalyst. Hydrogen evolves according to reactions (1) and (2): About 10 mL of hydrogen is generated by reaction (1) and about 56 mL of hydrogen is
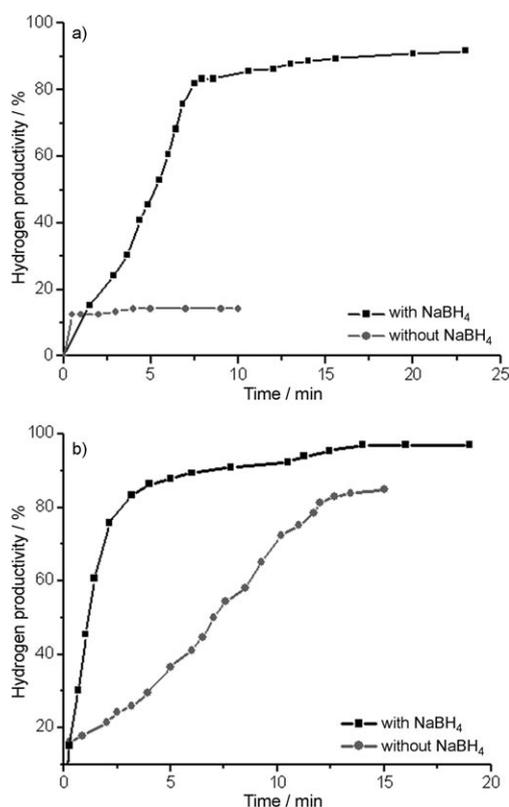
generated by reaction (2). Hence, the theoretical yield of hydrogen is 66 mL. The hydrogen productivity (experimental amount of H$_2$ produced/calculated H$_2$) from NaBH$_4$ and NH$_3$BH$_3$ catalyzed by Ni@SiO$_2$, Au@SiO$_2$, and Au–Ni@SiO$_2$ nanospheres is around 91.7, 83.3, and 97.0 % in 23, 143, and 14 min, respectively. It is clear that the Au–Ni@SiO$_2$ nanosphere is the most active of the three catalysts. Excluding experimental errors, the Au–Ni@SiO$_2$ catalyst generates a nearly stoichiometric amount of hydrogen in the hydrolysis of ammonia borane. The incomplete dehydrogenation catalyzed by the monometallic nanospheres is possibly a result of side-reactions that occur in addition to the hydrolysis of ammonia borane, as characterized by ^{11}B NMR spectroscopy of the reaction solution catalyzed by Au@SiO$_2$ (see the Supporting Information).[2b, 20]

$$NaBH_4 + 2H_2O \rightarrow Na^+ + BO_2^- + 4H_2 \qquad (1)$$

$$NH_3BH_3 + 2H_2O \rightarrow NH_4^+ + BO_2^- + 3H_2 \qquad (2)$$
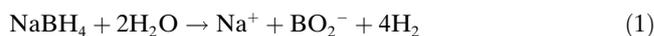
Clearly less hydrogen is generated by the side-reactions than by the hydrolysis of ammonia borane from the same amount of starting ammonia borane. It has been observed for many catalysts, for example, palladium black,[21a] platinum- and nickel-based alloys,[21b] and gold- and copper-based catalysts,[5c,21c] that less than a stoichiometric amount

of hydrogen is generated from the incomplete hydrolysis of ammonia borane.

In addition to the higher rate of generation and productivity of hydrogen, the Au–Ni@SiO$_2$ nanosphere also shows better durability than the monometallic catalysts. As shown in Figure 6, the yield of hydrogen decreases significantly for
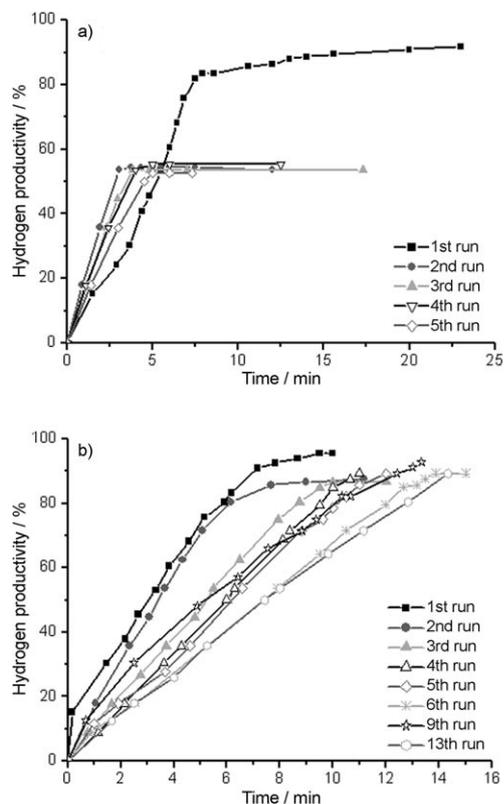

Figure 6. Hydrogen productivity vs. reaction time for the generation of hydrogen from an aqueous ammonia borane solution (0.152 M, 5 mL) catalyzed by the as-synthesized a) Ni@SiO$_2$ and b) Au–Ni@SiO$_2$ nanospheres at 18 °C in air after addition of the same amounts of AB.

the Ni@SiO$_2$ catalyst after the first run: The hydrogen productivity is reduced to around 50 % in the second cycle and remains at the same level in the following runs. In contrast, with Au–Ni@SiO$_2$, after the first cycle, the ability to generate hydrogen in the first several minutes is lowered slightly, but the final productivity remains at around 90 % even after 10 runs. These observations further demonstrate the regenerating function of the gold component for the catalyst.

The three catalysts were analyzed by powder XRD after the reaction (Figure 7). The nickel species could not be detected after the catalytic reaction, which indicates that the nickel NPs in Ni@SiO$_2$ are very small before and after the reaction, which was also confirmed by TEM observations (see the Supporting Information). In addition to the diffraction from the amorphous SiO$_2$ sphere, broad diffractions of $2\theta \approx 38.2°$ assigned to Au(111) were clearly detected in the Au@SiO$_2$ and Au–Ni@SiO$_2$ nanospheres, which indicates that the metal particles in the core were reduced to Au^0/Ni^0
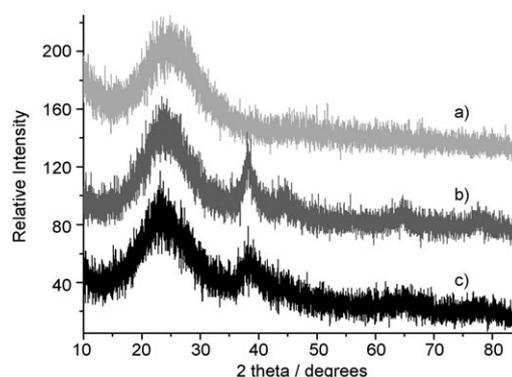

Figure 7. Powder XRD profiles for a) Ni@SiO$_2$, b) Au@SiO$_2$, and c) Au–Ni@SiO$_2$ nanospheres after the catalytic reaction.

and/or became larger after the catalytic reaction and were responsible for the XRD lines observed. The {111} diffraction of gold ($2\theta = 38.2°$) was clearly observable whereas that of fcc Ni–Au ($2\theta = 40.7°$) was absent from the Au–Ni@SiO$_2$ sample, which reveals that gold and nickel do not coexist as an alloy. Although the XRD patterns mainly provide information on larger particles, EDS and XPS analyses can give details of both large and small particles of Au–Ni. As discussed above, the EDS results indicate that gold and nickel coexist but are not separate in each spot/particle. Meanwhile, the XPS investigations show that Au–Ni is possibly phase-segregated but not an alloy as the nickel peak is not shifted to a lower energy than pure Ni^0 (852.7 eV; see below).[22] Moreover, we believe that most of the larger particles can be attributed to the aggregation of small particles; their compositions should be similar or the same. Therefore, all Au–Ni NPs in Au–Ni@SiO$_2$ are probably phase-segregated with Au–Ni interactions but not an Au–Ni alloy. Furthermore, compared with Au–Ni@SiO$_2$, in addition to the sharp diffraction at 38.2°, the other weaker characteristic peaks located at around 44.4, 64.6, and 77.7° for gold species could also be observed in the Au@SiO$_2$ sample. The results indicate that gold or Au–Ni NPs in Au–Ni@SiO$_2$ are smaller than gold NPs in Au@SiO$_2$ nanospheres and that the presence of nickel stabilizes gold NPs in a small size range during the reaction. TEM performed on the Au@SiO$_2$ and Au–Ni@SiO$_2$ nanospheres after catalytic reaction further confirmed the estimation based on powder XRD studies. Although most of the gold NPs in the Au@SiO$_2$ sample are in the range of 3–5 nm, quite a few gold NPs escape from the SiO$_2$ spheres to form very big agglomerations (over 10 nm) after the reaction (see the Supporting Information). As shown in the TEM images of Au–Ni@SiO$_2$ (Figure 8), the size of Au–Ni NPs located inside SiO$_2$ spheres remains constant after hydrogen generation, with very few agglomerations of Au–Ni NPs being found, as shown in Figure 8d, probably due to the splitting of a few SiO$_2$ spheres during the violent generation of hydrogen. Clearly there is less and slighter aggregation of particles in the core of Au–Ni@SiO$_2$ nanospheres than those in Au@SiO$_2$ nanospheres after reac-
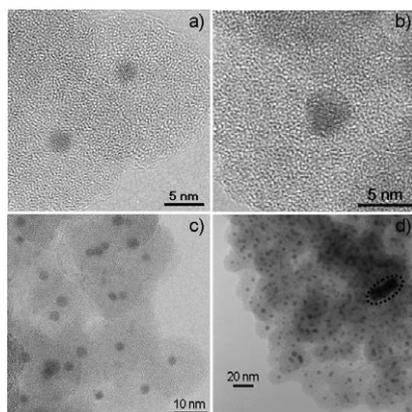
Figure 8. Representative high-magnification (a, b) and low-magnification (c, d) TEM images of Au–Ni@SiO$_2$ nanospheres after the catalytic reaction. The only agglomeration of Au–Ni NPs is highlighted by dashed black ellipse.

tion. Based on the facts described above, we assume that the broad gold diffractions observed at around 38.2° in Au–Ni@SiO$_2$ samples are not because of the growth of most Au–Ni NPs, but due to the appearance of a small quantity of aggregates of Au–Ni NPs.

X-ray photoelectron spectroscopy (XPS) on Au–Ni@SiO$_2$ nanospheres before and after reaction in combination with argon-sputtering were also performed to examine the structures of the Au–Ni NPs and to confirm the presence of gold and nickel inside the SiO$_2$ nanospheres (see the Supporting Information). The peak intensities of gold 4f and nickel 2p increase gradually with prolonged sputtering time. Moreover, the peaks from both gold and nickel become slightly stronger after hydrogen generation, possibly due to the few agglomerations of Au–Ni NPs after the reaction based on the TEM observations reported above. The silicon 2p and oxygen 1s bands of the Au–Ni@SiO$_2$ nanosphere before and after the reaction could be observed during the argon-sputtering, but the intensities clearly became weaker and weaker. Based on these observations, it can be concluded that the gold and nickel NPs are well coated by the SiO$_2$ nanospheres.

Conclusion

We have successfully prepared nickel, gold, and gold–nickel NPs with small diameters (3–4 nm for Au–Ni NPs) within silica nanospheres (around 15 nm) by using a reversed-micelle method. After in situ reduction in aqueous NaBH$_4$/NH$_3$BH$_3$ solution, nickel NPs in Ni@SiO$_2$ remain small whereas quite a few gold NPs in Au@SiO$_2$ readily aggregate, possibly due to their different surface energies. The nickel stabilizes the gold NPs to give Au–Ni NPs that remain small and form fewer agglomerations. Compared with monometallic nanospheres, the Au–Ni@SiO$_2$ catalyst exhibits superior performance in the hydrolytic dehydrogenation of ammonia borane in the following ways.

1) Au–Ni@SiO$_2$ presents the best activity in the generation of hydrogen, giving the greatest hydrogen productivity in the shortest time of all three catalysts, whereas Au@SiO$_2$ shows the lowest activity. The supported gold catalysts were shown to be less active for the hydrolytic dehydrogenation of ammonia borane, even the 2 nm gold NPs,[5c] which is usually regarded as the most active size.[23]

2) The hydrogen productivity of Ni@SiO$_2$ is greatly reduced after the first run, whereas it remains almost constant even after over 10 runs with the Au–Ni@SiO$_2$ catalyst.

3) As-synthesized Ni@SiO$_2$ is almost inactive for hydrogen generation without NaBH$_4$, whereas it has no great influence on the catalytic activity of Au–Ni@SiO$_2$ either in its presence or absence.

Based on the results described above, the synergetic effect between nickel and gold is very clear, not only benefiting the stability of Au–Ni NPs but also leading to high catalytic activity and recyclability. These findings are encouraging and could be extended to other systems or reactions, opening up a new avenue to high-performance catalysts in heterogeneous catalysis.

Experimental Section

Characterizations: The morphologies and sizes of all the samples were determined by using a transmission electron microscope (TEM, JEOL, JEM-3000F) equipped with an energy-dispersive X-ray detector (EDX) at an acceleration voltage of 300 kV. The dried powder samples were directly dispersed on a holey carbon film supported by a copper grid (Microgrid Type-A STEM150Cu, Okenshoji, Japan) without solvent and the whole procedure was carried out in air. Elemental analyses were performed on a Perkin–Elmer 2400 Series II analyzer. Powder X-ray diffraction (XRD) was performed on a RINT-2000 X-ray diffractometer with a Cu$_{K\alpha}$ source (40 kV, 40 mA). ^{11}B NMR spectra were recorded on a JEOL JNM-AL400 spectrometer operating at 128.15 MHz. Liquid samples of the filtrates, in which D$_2$O was included as a lock, were contained in sample tubes of 5 mm o.d. in which coaxial inserts of BF$_3$·(C$_2$H$_5$)$_2$O were placed as an external reference. The ^{11}B chemical shifts are given in δ units (parts per million) downfield from BF$_3$·(C$_2$H$_5$)$_2$O. The nitrogen sorption isotherms were measured by using an automatic volumetric adsorption equipment (Mircomeritics, ASAP 2010). Before the measurements, the sample were evacuated by using the "outgas" function of the surface area analyzer at room temperature until the outgas pressure reached 3 μmHg or below. X-ray photoelectron spectra were acquired with an ESCA-3400 spectrometer (Shimadzu Corp.) equipped with a Mg$_{K\alpha}$ X-ray exciting source (1253.6 eV) operating at 10 kV and 10 mA. The binding energies (BE) were referenced to the carbon 1s peak at 285.0 eV. After collecting the initial data, a 2 kV Ar$^+$ sputter beam was used for depth-profiling of the in situ synthesized samples.

Preparation of bis(ethylenediamine)gold(III) trichloride [Au(en)$_2$Cl$_3$]:[24] A solution of ethylenediamine (1.0 mL) in diethyl ether (5.0 mL) was slowly added to a solution of HAuCl$_4$·4H$_2$O (1.0 g) dissolved in diethyl ether (10 mL). The reaction proceeded to form a yellow precipitate, which was decanted. Then distilled water (2.8 mL) was added to dissolve the precipitate, which was again recovered as a pale-yellow precipitate by adding ethyl alcohol (20 mL). This solid was dissolved in distilled water (2.3 mL) and reprecipitated with ethyl alcohol (15 mL). The resulting pale solid was filtered and dried under vacuum overnight. Its purity was confirmed by powder XRD (see the Supporting Information).

Catalyst preparation: The Ni@SiO$_2$, Au@SiO$_2$, and Au–Ni@SiO$_2$ nanospheres were prepared in a similar manner by a reversed-micelle tech-

nique[19,25] as follows: Calculated amounts of aqueous solutions of $[Au(en)_2Cl_3]$ or/and $[Ni(NH_3)_6Cl_2]$ (typically 3.6 mL, the concentrations of $[Au(en)_2Cl_3]$ and $[Ni(NH_3)_6Cl_2]$ were 80 and 267 mmol L^{-1}, respectively) were rapidly injected into a cyclohexane solution of NP-5 (polyethylene glycol mono-4-nonylphenyl ether; 800 mL). The gold and nickel contents of the products ($Au/(Au+Ni+SiO_2)$ and $Ni/(Au+Ni+SiO_2)$) were theoretically determined from the concentrations of the metal ammine complexes to be 1.4 wt% in all the samples. After stirring at room temperature for about 15 h, an aqueous ammonia solution (28 wt%, 3.6 mL) was injected rapidly and after 2 h TEOS (tetraethoxysilane, $Si(OC_2H_5)_4$; 4.16 mL) was added rapidly. The solution was stirred for 2 days. The resulting solution was phase-separated by the addition of methanol, filtered, and washed with cyclohexane and acetone. After drying in a desiccator overnight, the solids obtained were used as as-synthesized catalysts. Elemental analyses found for Au@SiO$_2$: C 5.06, H 2.17, N 1.77; for Ni@SiO$_2$: C 2.55, H 1.67, N 3.31; for Au–Ni@SiO$_2$: C 3.73, H 1.89, N 4.13.

Procedure for the hydrolysis of ammonia borane: A mixture of sodium borohydride (NaBH$_4$, 5 mg), ammonia borane (NH$_3$BH$_3$, 26 mg, Sigma–Aldrich, 90%), and the catalyst (207.5 mg) was placed in a two-necked round-bottomed flask. One neck was connected to a gas burette and the other was connected to a pressure-equalization funnel to introduce distilled water (5 mL). The reaction started when distilled water was introduced into the mixture. The evolution of gas was monitored by using the gas burette (CAUTION! a certain ratio of air/H$_2$ could be explosive). For durability experiments, only NH$_3$BH$_3$ was added again. In the NaBH$_4$-free control experiments, only ammonia borane, catalyst, and distilled water were introduced. In addition, the molar ratio of Au/NH$_3$BH$_3$ and Ni/NH$_3$BH$_3$ were theoretically fixed at 0.019 and 0.065 for all the catalytic reactions. All the reactions were carried out at 18°C in air. Variations in the pH and temperature were monitored during the reactions in the presence of different catalysts (see the Supporting Information). The catalysts after reaction were centrifugally separated from the reaction solution and dried in air for characterization.

[1] a) L. Schlapbach, A. Züttel, *Nature* **2001**, *414*, 353–358; b) P. Chen, Z. Xiong, J. Luo, J. Lin, K. L. Tan, *Nature* **2002**, *420*, 302–304.

[2] a) N. L. Rosi, J. Eckert, M. Eddaoudi, D. T. Vodak, J. Kim, M. O'Keeffe, O. M. Yaghi, *Science* **2003**, *300*, 1127–1129; b) R. J. Keaton, J. M. Blacquiere, R. T. Baker, *J. Am. Chem. Soc.* **2007**, *129*, 1844–1845; c) C. W. Hamilton, R. T. Baker, A. Staubitzc, I. Manners, *Chem. Soc. Rev.* **2009**, *38*, 279–293.

[3] G. A. Deluga, J. R. Salge, L. D. Schmidt, X. E. Verykios, *Science* **2004**, *303*, 993–997.

[4] a) Z. Xiong, C. K. Yong, G. Wu, P. Chen, W. Shaw, A. Karkamkar, T. Autrey, M. O. Jones, S. R. Johnson, P. P. Edwards, W. I. F. David, *Nat. Mater.* **2008**, *7*, 138–141; b) A. Gutowska, L. Li, Y. Shin, C. M. Wang, X. S. Li, J. C. Linehan, R. S. Smith, B. D. Kay, B. Schmid, W. Shaw, M. Gutowski, T. Autrey, *Angew. Chem.* **2005**, *117*, 3644–3648; *Angew. Chem. Int. Ed.* **2005**, *44*, 3578–3582; c) T. He, Z. Xiong, G. Wu, H. Chu, C. Wu, T. Zhang, P. Chen, *Chem. Mater.* **2009**, *21*, 2315–2318.

[5] a) J. M. Yan, X. B. Zhang, S. Han, H. Shioyama, Q. Xu, *Angew. Chem.* **2008**, *120*, 2319–2321; *Angew. Chem. Int. Ed.* **2008**, *47*, 2287–2289; b) M. Chandra, Q. Xu, *J. Power Sources* **2006**, *159*, 855–860; c) M. Chandra, Q. Xu, *J. Power Sources* **2007**, *168*, 135–142.

[6] a) F. H. Stephens, R. T. Baker, M. H. Matus, D. J. Grant, D. A. Dixon, *Angew. Chem.* **2007**, *119*, 760–763; *Angew. Chem. Int. Ed.* **2007**, *46*, 746–749; b) M. E. Bluhm, M. G. Bradley, R. Butterick III, U Kusari, L. G. Sneddon, *J. Am. Chem. Soc.* **2006**, *128*, 7748–7749.

[7] a) Q. Xu, M. Chandra, *J. Power Sources* **2006**, *163*, 364–370; b) T. Umegaki, J. M. Yan, X. B. Zhang, H. Shioyama, N. Kuriyama, Q. Xu, *J. Power Sources* **2009**, *191*, 209–216; c) J. M. Yan, X. B. Zhang, S. Han, H. Shioyama, Q. Xu, *Inorg. Chem.* **2009**, *48*, 7389–7393.

[8] a) M. Haruta, T. Kobayashi, H. Sano, N. Yamada, *Chem. Lett.* **1987**, 405–408; b) M. Haruta, N. Yamada, T. Kobayashi, S. Iijima, *J. Catal.* **1989**, *115*, 301–309.

[9] a) M. Valden, X. Lai, D. W. Goodman, *Science* **1998**, *281*, 1647; b) F. Boccuzzi, A. Chiorino, M. Manzoli, P. Lu, T. Akita, S. Ichikawa, M. Haruta, *J. Catal.* **2001**, *202*, 256; c) G. Budroni, A. Corma, *Angew. Chem.* **2006**, *118*, 3406–3409; *Angew. Chem. Int. Ed.* **2006**, *45*, 3328–3331.

[10] a) B. Solsona, M. Conte, Y. Cong, A. Carley, G. Hutchings, *Chem. Commun.* **2005**, 2351–2353; b) A. Wolf, F. Schüth, *Appl. Catal. A* **2002**, *226*, 1–13.

[11] M. M. Schubert, S. Hackenberg, A. C. van Veen, M. Muhler, V. Plzak, R. J. Behm, *J. Catal.* **2001**, *197*, 113–122.

[12] C.-W. Chiang, A. Wang, B.-Z. Wan, C.-Y. Mou, *J. Phys. Chem. B* **2005**, *109*, 18042–18047.

[13] M. Bandyopadhyay, O. Korsak, M. W. E. van den Ber, W. Grünert, A. Birkner, W. Li, F. Schüth, H. Gies, *Microporous Mesoporous Mater.* **2006**, *89*, 158–163.

[14] C.-M. Yang, M. Kalwei, F. Schüth, K.-J. Chao, *Appl. Catal. A* **2003**, *254*, 289–296.

[15] a) W. Yan, S. M. Mahurin, B. Chen, S. H. Overbury, S. Dai, *J. Phys. Chem. B* **2005**, *109*, 15489–15496; b) K. Qian, H. Sun, W. Huang, J. Fang, S. Lv, B. He, Z. Jiang, S. Wei, *Chem. Eur. J.* **2008**, *14*, 10595–10602.

[16] a) X. Liu, A. Wang, X. Wang, C. Mou, T. Zhang, *Chem. Commun.* **2008**, 3187–3189; b) S. Zhou, H. Yin, V. Schwartz, Z. Wu, D. Mullins, B. Eichhorn, S. H. Overbury, S. Dai, *ChemPhysChem* **2008**, *9*, 2475–2479.

[17] a) F. Caruso, M. Spasova, V. Salgueiriño-Maceira, L. M. Liz-Marzán, *Adv. Mater.* **2001**, *13*, 1090–1094; b) M. Kim, K. Sohn, H. B. Na, T. Hyeon, *Nano Lett.* **2002**, *2*, 1383–1387; c) Y. Lu, Y. D. Yin, Z.-Y. Li, Y. N. Xia, *Nano Lett.* **2002**, *2*, 785–788.

[18] a) V. S. Murthy, J. N. Cha, G. D. Stucky, M. S. Wong, *J. Am. Chem. Soc.* **2004**, *126*, 5292–5299; b) S. Liu, M. Han, *Adv. Funct. Mater.* **2005**, *15*, 961–967; c) P. M. Arnal, M. Comotti, F. Schüth, *Angew. Chem.* **2006**, *118*, 8404–8407; *Angew. Chem. Int. Ed.* **2006**, *45*, 8224–8227; d) J. Lee, J. C. Park, H. Song, *Adv. Mater.* **2008**, *20*, 1523–1528.

[19] T. Miyao, N. Toyoizumi, S. Okuda, Y. Imai, K. Tajima, S. Naito, *Chem. Lett.* **1999**, 1125–1126.

[20] a) F. H. Stephens, V. Pons, R. T. Baker, *Dalton Trans.* **2007**, 2613–2626; b) M. C. Denney, V. Pons, T. J. Hebden, D. Michael Heinekey, K. I. Goldberg, *J. Am. Chem. Soc.* **2006**, *128*, 12048–12049.

[21] a) M. Chandra, Q. Xu, *J. Power Sources* **2006**, *156*, 190–194; b) C. F. Yao, L. Zhuang, Y. L. Cao, X. P. Ai, H. X. Yang, *Int. J. Hydrogen Energy* **2008**, *33*, 2462–2467; c) S. B. Kalidindi, U. Sanyal, B. R. Jagirdar, *Phys. Chem. Chem. Phys.* **2008**, *10*, 5870–5874.

[22] J. L. Rousset, F. J. Cadete Santos Aires, B. R. Sekhar, P. Mélinon, B. Prevel, M. Pellarin, *J. Phys. Chem. B* **2000**, *104*, 5430–5435.

[23] a) M. Haruta, *Chem. Rec.* **2003**, *3*, 75–87; b) H. Falsig, B. Hvolbæk, I. S. Kristensen, T. Jiang, T. Bligaard, C. H. Christensen, J. K. Nørskov, *Angew. Chem.* **2008**, *120*, 4913–4917; *Angew. Chem. Int. Ed.* **2008**, *47*, 4835–4839.

[24] a) B. P. Block, J. C. Bailar, *J. Am. Chem. Soc.* **1951**, *73*, 4722–4725; b) R. C. Elder, J. W. Watkins II, *Inorg. Chem.* **1986**, *25*, 223–226; c) H. Zhu, C. Liang, W. Yan, S. H. Overbury, S. Dai, *J. Phys. Chem. B* **2006**, *110*, 10842–10848; d) T. Ishida, K. Kuroda, N. Kinoshita, W. Minagawa, M. Haruta, *J. Colloid Interface Sci.* **2008**, *323*, 105–111.

[25] a) A. J. Zarur, J. Y. Ying, *Nature* **2000**, *403*, 65–67; b) S.-J. Cho, J.-C. Idrobo, J. Olamit, K. Liu, N. D. Browning, S. M. Kauzlarich, *Chem. Mater.* **2005**, *17*, 3181–3186; c) S. Naito, K. Minoshima, T. Miyao, *Top. Catal.* **2006**, *39*, 131–136.